Third-order optical nonlinearity of one-dimensional Dirac fermions

Ze Zheng,[1,2] Ming Rui Zhang,[3] and Jin Luo Cheng[1,2,*]

[1]*GPL Photonics Lab, State Key Laboratory of Applied Optics, Changchun Institute of Optics, Fine Mechanics and Physics, Chinese Academy of Sciences, Changchun 130033, China*
[2]*School of Physical Sciences, University of Chinese Academy of Sciences, Beijing 100039, China*
[3]*Department of Physics, University of Jilin, Changchun 130015, China*

The optical nonlinearity of Dirac fermions in two and three dimensions show unique properties determined by analytic expressions in the independent particle approximation, which promotes their host materials as potential candidates for providing optical nonlinear functionalities. In this work we theoretically study the third-order optical nonlinearity for one-dimensional Dirac fermions and obtain analytical expressions for third-order optical conductivities at general light frequencies. The conductivity includes many resonant peaks induced by the resonant optical transitions associated with intraband motion as well as one-, two-, and three-photon interband processes. The conductivities for field-induced second harmonic generation and third harmonic generation are discussed in detail. To connect with real materials, we choose armchair graphene nanoribbons, which host one-dimensional Dirac fermions for its low energy electronic excitation, and our analytical expressions are applied to get the third-order conductivity for harmonic generations with different ribbon width. By comparing with numerical results evaluated from a full band structure in a tight binding model, the analytic and numerical results agree pretty well for photon energy below 2.5 eV.

I. INTRODUCTION

Dirac fermions (DFs) have attracted much attention in various research fields after their discovery in crystals, mostly ascribed to the unique linear dispersions [1–6]. Nowadays many properties of DFs that have been well studied in high energy physics can be experimentally demonstrated in solids much easier, which also inspires new research fields in nontrivial topological materials. DFs can be realized in the low energy electronic excitations of different dimensions: graphene [1,7–9], twisted bilayer graphene [10–12], transition metal dichalcogenides [13–15], and surface states of topological insulators [16,17] for two dimensional (2D) DFs; Dirac semimetals [4,18,19] and Weyl semimetals [3,5,20] for three dimensional (3D) DFs; and nanoribbons, nanotubes, nanorings [21–25], SSH model of polyacetylene [6,26], and edge states of 2D topological insulators [27,28] for one-dimensional (1D) DFs. DFs exhibit unique and remarkable optical properties, including the universal conductance [29,30], broadband absorption from terahertz wavelength to visible light [31,32], extremely strong optical nonlinearities [9,33–37], and easy tunability either by external field [38–41] or by thickness [42,43]; their host materials become potential candidates for applications in optoelectronics and nonlinear photonics.

The optical nonlinearities of 2D and 3D DFs have been extensively studied [9,44], and huge nonlinear conductivities are both theoretically predicted [35,45,46] for general light frequencies and experimentally demonstrated [39,47] in various nonlinear optical phenomena. The nonlinear optical conductivities of massless 3D DFs can be calculated by integrating those of 2D DFs over the mass [48], and they show many similarities in the spectra, including the huge susceptibility that is orders of magnitude larger than usual semiconductors or insulators [49], the existence of many resonances induced by both intraband motion for involved photon energies approaching zero [50,51] and interband transitions for involved photon energies matching the chemical potential induced gap [36], and the easy tunability by the chemical potential [52]. Furthermore, their spectra show almost the same fine structures. However, the quantum confinement also leads to significant differences between 2D and 3D DFs: (1) the effective third-order optical conductivities of 2D DFs are in general two orders of magnitude larger than that of 3D DFs, (2) they have different dependence on the Fermi velocity, and (3) they show different chemical potential dependence. It is interesting to understand how the optical nonlinearities behave with further reducing the dimension to 1D, which is the focus of this work.

In this paper we study the third-order nonlinear response for 1D DFs. The expressions of perturbative conductivities are obtained from the perturbation solution of equation of motion with describing the light matter interaction in the length gauge [53]. Further, the electronic states of 1D DFs are described by an effective Hamiltonian linearly depending on the wave vector. In this model, the expressions for linear and third-order conductivities can be analytically worked out for arbitrary light frequencies, and based on them we give a detailed discussion on the electric-field-induced second

*jlcheng@ciomp.ac.cn

harmonic generation (EFISH) and third harmonic generation (THG). To connect with real materials, we find that the low energy electronic excitations of armchair graphene nanoribbons can be well described by 1D DFs. EFISH and THG of armchair graphene nanoribbons are calculated by two methods: (1) the analytical expressions obtained from the effective model of 1D DFs and (2) a direct numerical evaluation where the electronic states of the ribbons are described by a tight binding model; both methods show good agreement for photon energy less than 2.5 eV. With changing the dimension, new control methods can be introduced to tune the nonlinear response. Compared to graphene, for 3D DFs the thickness of its host materials is a good control variable, which allows a flexible structure design toward realizing the device nonlinear functionalities; while for 1D DFs, a patterned array of nanoribbons can provide an extra degree of freedoms, including the period and the coverage rate, in possible devices. The precondition for such application requires understanding of

the optical nonlinearity of 1D DFs in a similar way compared to that of 2D and 3D DFs.

In Sec. II we give the effective Hamiltonian as well as the expressions for linear and third-order optical conductivities. In Sec. III we discuss the general properties of these expressions and the spectra of harmonic generations. In Sec. IV the analytic expressions are compared with the numerical results for armchair graphene nanoribbons. In Sec. V, we discuss and conclude.

II. MODELS

A. Effective Hamiltonian for 1D Dirac fermions

The effective Hamiltonian for 1D DFs is written as [54]

$$H_k = \hbar v_F(k\sigma_x + q\sigma_z), \tag{1}$$

where v_F is the Fermi velocity, $\hbar v_F q$ is a mass term, and $\sigma_{x,y}$ are Pauli matrices. The velocity operator is

$$v_k = \hbar^{-1}\partial_k H_k = v_F\sigma_x. \tag{2}$$

The eigenstates and eigenenergies of H_k are

$$\psi_{+k} = \frac{1}{\sqrt{2}}\begin{pmatrix} \sqrt{1+\mathcal{N}_k} \\ \sqrt{1-\mathcal{N}_k}\,\mathrm{sgn}(k) \end{pmatrix}, \quad \varepsilon_{+k} = +\hbar v_F\epsilon_k, \tag{3}$$

$$\psi_{-k} = \frac{1}{\sqrt{2}}\begin{pmatrix} -\sqrt{1-\mathcal{N}_k}\,\mathrm{sgn}(k) \\ \sqrt{1+\mathcal{N}_k} \end{pmatrix}, \quad \varepsilon_{-k} = -\hbar v_F\epsilon_k, \tag{4}$$

with the band index $s = \pm$, $\epsilon_k = \sqrt{k^2 + q^2}$ and $\mathcal{N}_k = q/\epsilon_k$. For the latter use we give the velocity matrix elements

$$v_{ssk} = sv_F\frac{k}{\epsilon_k}, \quad v_{s\bar{s}} = v_F\frac{q}{\epsilon_k}, \tag{5}$$

and the matrix elements of Berry connections

$$\xi_{s_1 s_2 k} \equiv \psi_{s_1 k}^\dagger i\partial_k\psi_{s_2 k} = \delta_{s_1\bar{s}_2}is_2\frac{q}{2\epsilon_k^2}, \tag{6}$$

where $\bar{s}$ represents the index of the band distinguished from the s band.

B. Linear and third-order optical conductivities

Using the electronic states described above and following Ref. [53], we first set up equation of motion with describing the light matter interaction in a length gauge, then we perturbatively solve the density matrix at different power orders of light fields, and finally we obtain the formulas for linear and third-order optical conductivities, which are the same as those presented in Appendix A of Ref. [53] with taking the directions of both the electric field and the current along the x direction. For the effective model of 1D DFs discussed in the previous section, these formulas depend on the electron eigen energies in Eqs. (3) and (4), the velocity matrix elements in Eq. (5), and the Berry connection in Eq. (6); they can be worked out analytically. The linear conductivity is then

$$\sigma^{(1)}(\omega) = \frac{ie^2 v_F}{\pi E_q}S_l\left(\frac{\hbar\omega + i\Gamma_a^{(1)}}{E_q}, \frac{\hbar\omega + i\Gamma_e^{(1)}}{E_q}, \frac{2|\mu|}{E_q}\right), \tag{7}$$

where $E_q = 2\hbar v_F|q|$ is the band gap, μ is the chemical potential, and $\Gamma_{a/e}^{(1)}$ are the phenomenological relaxation energy parameter for intraband/interband transition in the linear response. The dimensionless function S_l is

$$S_l(v, w, u) = \frac{1}{v}\frac{\sqrt{u^2 - 1}}{u}\theta(u - 1) + \frac{I_2(g)}{w} + \frac{G(g; w)}{2w^2}, \tag{8}$$

with $g = \max\{1, u\}$, and

$$I_2(g) = \frac{1}{g^2 + g\sqrt{g^2 - 1}}, \tag{9}$$

$$G(g; w) = \frac{1}{\sqrt{w^2 - 1}} \ln\left(-\frac{\sqrt{w^2 - 1} + w}{\sqrt{w^2 - 1} - w} \times \frac{w - g}{w + g} \times \frac{\sqrt{w^2 - 1}\sqrt{g^2 - 1} - 1 - wg}{\sqrt{w^2 - 1}\sqrt{g^2 - 1} - 1 + wg}\right). \tag{10}$$

Note that the logarithmic function is taken as $\ln(x + iy) = \ln\sqrt{x^2 + y^2} + i[\frac{\pi}{2}\mathrm{sgn}(y) - \arctan\frac{x}{y}]$. The third-order conductivity is expressed as

$$\sigma^{(3)}(\omega_1, \omega_2, \omega_3) = \frac{1}{6}[\tilde{\sigma}^{(3)}(\omega, \omega_2 + \omega_3, \omega_3) + \tilde{\sigma}^{(3)}(\omega, \omega_2 + \omega_3, \omega_2) + \tilde{\sigma}^{(3)}(\omega, \omega_1 + \omega_3, \omega_3)$$

$$+ \tilde{\sigma}^{(3)}(\omega, \omega_1 + \omega_3, \omega_1) + \tilde{\sigma}^{(3)}(\omega, \omega_1 + \omega_2, \omega_1) + \tilde{\sigma}^{(3)}(\omega, \omega_1 + \omega_2, \omega_2)], \tag{11}$$

with $\omega = \omega_1 + \omega_2 + \omega_3$ and the unsymmetrized conductivity $\tilde{\sigma}^{(3)}(\omega, \omega_0, \omega_3)$ giving as

$$\tilde{\sigma}^{(3)}(\omega, \omega_0, \omega_3) = \frac{ie^4\hbar^2 v_F^3}{2\pi}\frac{4}{E_q^5}S_{nl}\left(\frac{\hbar\omega + i\Gamma_a^{(3)}}{E_q}, \frac{\hbar\omega_0 + i\Gamma_a^{(2)}}{E_q}, \frac{\hbar\omega_3 + i\Gamma_a^{(1)}}{E_q};\right.$$

$$\left.\frac{\hbar\omega + i\Gamma_e^{(3)}}{E_q}, \frac{\hbar\omega_0 + i\Gamma_e^{(2)}}{E_q}, \frac{\hbar\omega_3 + i\Gamma_e^{(1)}}{E_q}; \frac{2|\mu|}{E_q}\right). \tag{12}$$

Here ω_0 stands for the sum of any two photon energies and $\Gamma_{a/e}^{(2/3)}$ are phenomenological relaxation parameters for the second/third-order transition processes. The dimensionless function S_{nl} is

$$S_{nl}(v, v_0, v_3; w, w_0, w_3; u) = \theta(u - 1)\frac{\sqrt{u^2 - 1}}{u^5}\left[\frac{6}{vv_0v_3} + \frac{S_3(w_0; u)}{vv_3} + \frac{S_5(w; u)}{v_0v_3} + \frac{S_7(w, w_0; u)}{v_3} + S_{8a}(w, w_0, w_3; u)\right]$$

$$+ \frac{S_2(w_3; g)}{vv_0} + \frac{S_4(w_0, w_3; g)}{v} + \frac{S_6(w, w_3; g)}{v_0} + S_{8b}(w, w_0, w_3; g). \tag{13}$$

All dimensionless functions S_j can be obtained analytically and are given in Appendix.

III. RESULTS

A. General properties

We first discuss some general properties of the linear conductivity in Eq. (7) and the third-order conductivity in Eq. (11). In the perturbative treatment, the optical transitions include the intraband and interband transitions. For the linear conductivity, the first term of S_l in Eq. (8) gives the contribution from the intraband transition, and the remaining terms originate from the interband transitions. As one expects, the intraband transition gives the Drude term which is nonzero only for a doped system $u > 1$. For the third-order conductivity in Eq. (13), besides that the term $\propto \frac{1}{vv_0v_3}$ is purely from intraband transitions and the terms S_{8a} and S_{8b} are purely from interband transitions, all other terms are mixtures of both transitions. We consider several general cases in certain limits.

(1) In the clean limit, there exist multiple divergences in Eq. (7) for linear conductivity and in Eq. (11) for third-order conductivity, which become resonant peaks with the inclusion of scatterings. These divergences are induced either by interband transitions associated with one-, two-, and three-photon processes, or by intraband motion. The interband resonances are identified by the function $G(g, w)$, with a singularity point at $w = g$, which gives resonant conditions $\hbar\omega/E_q = g$ for one-photon process [left arrows in Fig. 1(a)] with gE_q being the effective band gap, $(\hbar\omega_i + \hbar\omega_j)/E_q = g$ with $i \neq j$ for two-photon process [right arrows in Fig. 1(a)], and $(\hbar\omega_1 +$

$\hbar\omega_2 + \hbar\omega_3)/E_q = g$ for three-photon process [Fig. 1(b)]. The interband resonance diverges as a logarithmic function. The intraband motion-induced divergences arise from the Drude-like contribution and occur at $v_3 = 0$, $v_0 = 0$, or $v = 0$, illustrated in Figs. 1(c) and 1(d). Around these singularities, the value of the conductivity sensitively depends on the relaxation parameters and the realistic scattering processes are important. These resonances are similar to that in 2D and 3D DFs [9,48,53].

(2) As the gap $E_q \to 0$, the conductivities are approximated as

$$\sigma^{(1)}(\omega) \approx \frac{ie^2 v_F}{\pi(\hbar\omega + i\Gamma_a^{(1)})}, \tag{14}$$

$$\sigma^{(3)}(\omega_1, \omega_2, \omega_3) \propto O(E_q^2). \tag{15}$$

In this limit, only the Drude term in the linear conductivity survives and gives a chemical potential independent value, while the third-order conductivity vanishes. This can be understood as following: because the optical transition between these two bands is proportional to the gap parameter E_q as shown in Eq. (6), there is no interband optical transition at zero gap $E_q = 0$, and the electrons can move only inside one band. For 1D DFs, the intraband movement of the electron has a constant velocity. Therefore, as long as it moves inside one band, the current does change, which cannot induce any optical nonlinearity. Different from DFs at higher dimensions, the third-order optical nonlinearity for 1D DFs only exists for a gapped system.
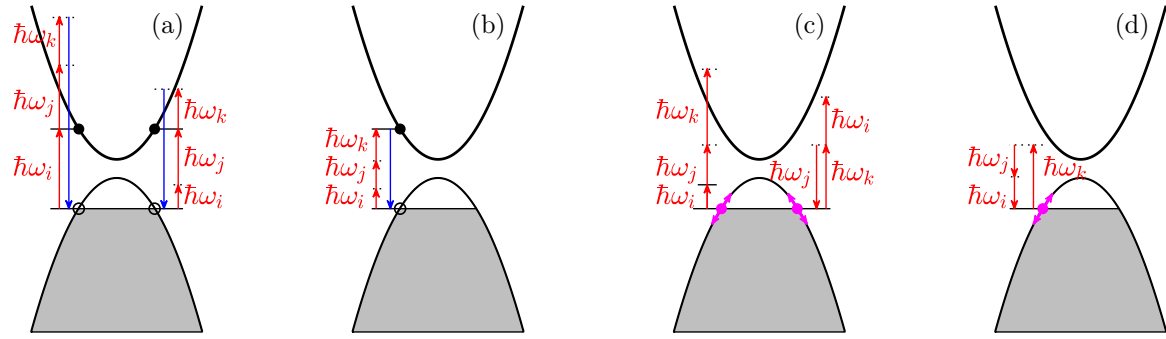
FIG. 1. Illustration of the resonant transitions in third-order optical nonlinearity. (a) One-photon interband resonant process (left) and two-photon interband resonant process (right), (b) Three-photon interband resonant process, (c) One-photon intraband resonant process with $\hbar\omega_i = 0$ (left) and two-photon intraband resonant process with $\hbar\omega_j + \hbar\omega_k = 0$ (right), and (d) Three-photon intraband resonant process with $\hbar\omega_i + \hbar\omega_j + \hbar\omega_k = 0$.

(3) The responses at very low photon energies can be revealed by the limits of $\sigma^{(1)}(x\omega)$ and $\sigma^{(3)}(x\omega_1, x\omega_2, x\omega_3)$ with taking $x \to 0$. With all damping parameters approaching zero, we get

$$\sigma^{(1)}(\omega) \approx \begin{cases} \frac{ie^2 v_F}{\pi} \frac{\sqrt{4\mu^2 - E_q^2}}{2\mu\hbar\omega} & 2|\mu| > E_q, \\ -\frac{ie^2 v_F}{\pi} \frac{2\hbar\omega}{3E_q^2} & 2|\mu| < E_q, \end{cases} \quad (16)$$

and

$$\sigma^{(3)}(\omega_1, \omega_2, \omega_3) \approx \begin{cases} \frac{ie^4 \hbar^2 v_F^3}{2\pi} \frac{E_q^2 \sqrt{4\mu^2 - E_q^2}}{8\hbar^3 \omega_1 \omega_2 \omega_3 |\mu|^5} & 2|\mu| > E_q, \\ -\frac{ie^4 \hbar^2 v_F^3}{2\pi} \frac{256\hbar(\omega_1 + \omega_2 + \omega_3)}{45 E_q^6} & 2|\mu| < E_q. \end{cases} \quad (17)$$

When the system is doped for $2|\mu| > E_q$, only the intraband contributions remain for both the linear and third-order conductivities, giving the frequency dependence ω^{-1} and $(\omega_1 \omega_2 \omega_3)^{-1}$, respectively. This is similar to the results in doped 2D or 3D DFs, but the optical conductivities show different dependencies on the chemical potential and Fermi velocity. While as the system is undoped $2|\mu| < E_q$, the conductivities are linear with the frequencies, which gives zero conductivities at zero frequencies but finite susceptibility.

(4) Table I gives a comparison on the features for the linear and third-order optical conductivities at different dimensions. The most direct effect of the dimension is the Fermi velocity dependence, which gives $\propto v_F^{2-n}$ for linear conductivity and $\propto v_F^{4-n}$ for third-order conductivity in n dimension. At small photon energies, the responses have the same frequency dependence, but different chemical potential and gap parameter dependencies. Interestingly, when there exists a real gap

$E_q > 2|\mu| > 0$, the conductivities at low photon energies are proportional to the frequencies and inversely proportional to a power of the gap parameter with the power index depending on the dimension; for the chemical potential induced gap $2\mu > E_q$, the Drude-like contribution gives the conductivities inversely depending on the frequencies. When the frequencies are much higher than the effective gap, the frequency dependencies of these conductivities vary with the dimension. These features might be used to identify the dimension of the DFs.

B. Harmonic generations

As an illustration of these results, we give the spectra of the linear conductivity $\sigma^{(1)}(\omega)$, $\sigma^{(3)}(\omega, \omega, 0)$ for EFISH, and $\sigma^{(3)}(\omega, \omega, \omega)$ for THG at different chemical potentials. Because armchair graphene nanoribbons are centrosymmetric, there is no SHG in the electric dipole approximation. However, applying a static electric field along the ribbon direction can break the inversion symmetry and make it to be SHG active (usually called as EFISH), which indeed is a third-order optical process with taking one of the incident frequencies as zero. After writing these conductivities as

$$\sigma^{(1)}(\omega) = \frac{e^2 v_F}{\pi E_q} \mathcal{S}_1 \left(\frac{\hbar\omega}{E_q}, \frac{2|\mu|}{E_q} \right), \quad (18)$$

$$\sigma^{(3)}(\omega, \omega, 0) = \frac{2e^4 \hbar^2 v_F^3}{\pi E_q^5} \mathcal{S}_{\text{SHG}} \left(\frac{\hbar\omega}{E_q}, \frac{2|\mu|}{E_q} \right), \quad (19)$$

$$\sigma^{(3)}(\omega, \omega, \omega) = \frac{2e^4 \hbar^2 v_F^3}{\pi E_q^5} \mathcal{S}_{\text{THG}} \left(\frac{\hbar\omega}{E_q}, \frac{2|\mu|}{E_q} \right), \quad (20)$$

TABLE I. Comparison of some features for the optical conductivities $\sigma^{(1);xx}(\omega)$ and $\sigma^{(3);xxxx}(\omega_1, \omega_2, \omega_3)$ at different dimensions with respect to the Fermi velocity v_F, the frequency ω or ω_i, the chemical potential μ, and the mass term E_q. Here $E_g = \max\{E_q, 2|\mu|\}$, $\Delta = E_q/2$, "–" indicates unavailable or too complicated to be specified, "*" indicates for $\sigma^{(3);xxxx}(\omega, \omega, \omega)$, $\omega_{ij} = \omega_i + \omega_j$, and $\omega_{123} = \omega_1 + \omega_2 + \omega_3$.

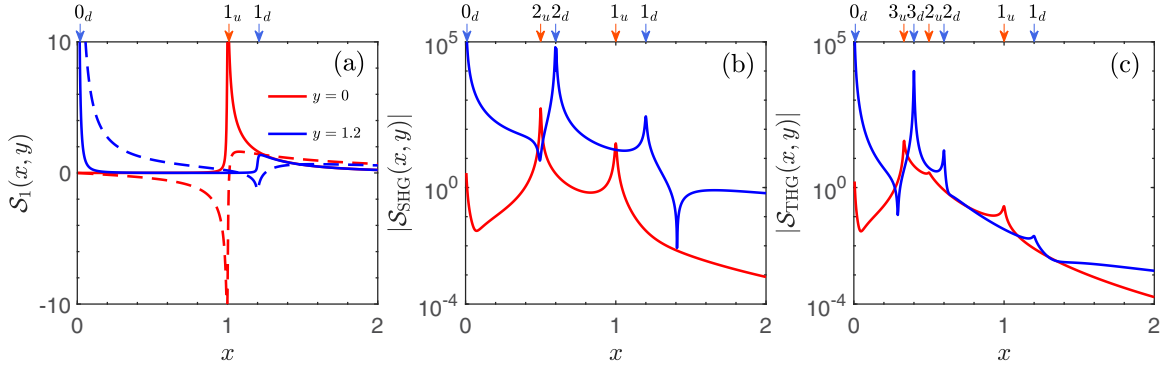| Dimension	v_F		$\hbar\omega \ll E_g = 2|\mu|$		$\hbar\omega \ll E_g = E_q$		$\hbar\omega \gg E_g$	
	$\sigma^{(1)} \propto$	$\sigma^{(3)} \propto$	$\sigma^{(1)} \propto$	$\sigma^{(3)} \propto$	$\sigma^{(1)} \propto$	$\sigma^{(3)} \propto$	$\sigma^{(1)} \propto$	$\sigma^{(3)} \propto$
1D	v_F	v_F^3	$\frac{\sqrt{\mu^2 - \Delta^2}}{|\mu|\omega}$	$\frac{\Delta^2 \sqrt{\mu^2 - \Delta^2}}{|\mu|^5 \omega_1 \omega_2 \omega_3}$	$\frac{\omega}{\Delta^2}$	$\frac{\omega_1 + \omega_2 + \omega_3}{\Delta^6}$	$\frac{1}{\omega}$	–
2D [36]	1	v_F^2	$(1 - \frac{\Delta^2}{\mu^2})\frac{|\mu|}{\omega}$	$\frac{(\mu^2 - \Delta^2)(\mu^2 + 3\Delta^2)}{\omega_1 \omega_2 \omega_3 |\mu|^5}$	$\frac{\omega}{\Delta}$	$\frac{\omega_1 + \omega_2 + \omega_3}{\Delta^5}$	1	$\frac{1}{\omega_{12} \omega_{23} \omega_{31} \omega_{123}}$
3D [48]	$\frac{1}{v_F}$	v_F	$\frac{|\mu|^2}{\omega}$	$\frac{1}{\omega_1 \omega_2 \omega_3}$	–	–	$\frac{\omega}{|\mu|} \ln \frac{\omega}{|\mu|}$	$\frac{1}{\omega^3}$ *

FIG. 2. Spectra of (a) linear conductivity $\mathcal{S}_1(x, y)$, its real and imaginary parts are given by solid and dashed curves, respectively; (b) $|\mathcal{S}_{\mathrm{SHG}}(x, y)|$ for EFISH and (c) $|\mathcal{S}_{\mathrm{THG}}(x, y)|$ for THG at chemical potentials $y = 0$ (red lines) and $y = 1.2$ (blue lines). Arrows with labels $i_{d/u}$ for $i = 1, 2, 3$ indicate the position of i-photon interband resonant peaks for undoped ("u") and doped ("d") case; arrows 0_d indicate the intraband resonant peaks for a doped case. The intraband and interband relaxation parameters are all $\Gamma_{a/e}^{(n)} = 0.01 E_q$.

these dimensionless functions $\mathcal{S}_1(x, y)$, $|\mathcal{S}_{\mathrm{SHG}}(x, y)|$, and $|\mathcal{S}_{\mathrm{THG}}(x, y)|$ are plotted in Fig. 2 for $2|\mu|/E_q = 0$ and 1.2 with taking all $\Gamma_{a/e}^{(i)}/E_q = 0.01$. The interband resonant peaks appear at $\hbar\omega = E_g$ for one-photon resonant transition (indicated by arrows 1_d, 1_u), $E_g/2$ for two-photon resonant transition (indicated by arrows 2_d, 2_u), and $E_g/3$ for three-photon resonant transition (indicated by arrows 3_d, 3_u) with $E_g = \max\{2|\mu|, E_q\}$ for both doped and undoped cases, while the intraband resonant peaks (indicated by arrows 0_d) appear at $\hbar\omega = 0$ only for doped case. All these results agree with

our discussion on the analytic expression of the conductivity in previous sections.

IV. COMPARISON WITH THE OPTICAL RESPONSE OF ARMCHAIR GRAPHENE NANORIBBONS

For armchair graphene nanoribbons with N dimers in one unit as shown in Fig. 2(a), a simple tight binding Hamiltonian and position operator can be written as [55]

$$H_k = \gamma_0 \begin{pmatrix} 0 & F_k \\ F_k^\dagger & 0 \end{pmatrix}, \tag{21}$$

$$X_k = \begin{pmatrix} A_k & 0 \\ 0 & A_k + \frac{a_0}{3} \end{pmatrix}, \tag{22}$$

where the block matrix F_k has matrix elements $F_{nmk} = \delta_{n,m} + \delta_{n,m+1} + e^{-ika_0}\delta_{n+1,m}$ for $1 \leqslant n, m \leqslant N$ with $\gamma_0 = 2.7\,\mathrm{eV}$ and $a_0 = \sqrt{3}a_{\mathrm{gh}} = \sqrt{3} \times 2.46\,\text{Å}$ being the lattice constant, and the matrix elements of position operator are given by $A_{nmk} = \delta_{nm}\frac{n-1}{2}a_0$. The velocity operator is

$$v_k = \frac{1}{i\hbar}[X_k, H_k] + \frac{1}{\hbar}\partial_k H_k. \tag{23}$$

The Hamiltonian in Eq. (21) can be diagonalized analytically with the eigen energies [55]

$$\varepsilon_{snk} = s\gamma_0 \sqrt{1 - 4\cos\left(\frac{ka_0}{2}\right)\cos\left(\frac{n}{N+1}\pi\right) + 4\cos^2\left(\frac{n}{N+1}\pi\right)}, \quad \text{for } s = \pm; n = 1, \cdots, N; \text{ and } k \in [-\pi/a_0, \pi/a_0). \tag{24}$$

Note that the band index n does not correspond to the energy order of the bands at $k = 0$. The band structures for $N = 3$ and $N = 4$ are plotted in Figs. 3(b) and 3(c), and there exist two flat bands $\pm\frac{N+1}{2}$ for odd number N. The velocity matrix elements are nonzero only between the band pair $\pm n$, indicating that the optical transitions only occur between these band pairs. Furthermore, we also find that the bands m and $N + 1 - m$ can be connected smoothly to form one band (indexed by m) with double the size of Brillouin zone, as giving by the solid curves in Figs. 3(b) and 3(c). Then as $1 \leqslant n < N/2$, these band pairs $\pm n$ around $k = 0$ can be approximated by the 1D DFs with mass energy and Fermi

velocity

$$E_q = 2\gamma_0 \left| 2\cos\left(\frac{n}{N+1}\pi\right) - 1 \right|,$$

$$v_F = \sqrt{2\cos\left(\frac{n}{N+1}\pi\right)} \frac{\sqrt{3}a_0\gamma_0}{2\hbar}. \tag{25}$$

Around the band edge of these band pairs, their optical conductivities can be approximately evaluated by using our analytic expressions in Eq. (11).
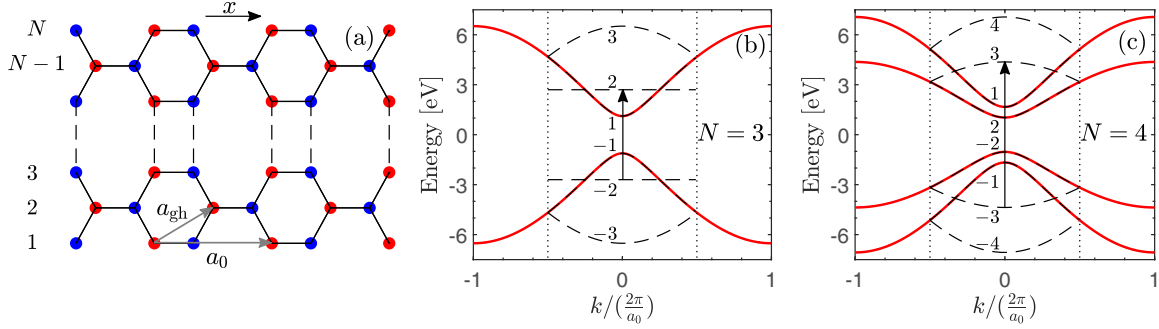
FIG. 3. (a) Illustration of a N-armchair graphene nanoribbon, the x direction is along the armchair direction. Black dashed curves are the band structure in one Brillouin zone for (b) $N = 3$ and (c) $N = 4$. The red solid curves give the unfolded bands in an extended Brillouin zone. The band indexes are shown around the position $k = 0$.

With the velocity matrix elements and eigen energies, third-order conductivities for EFISH and THG in graphene nanoribbons can be numerically calculated using the full perturbative expressions in Refs. [53]. Here we first perform the calculation for $N = 3$ and $N = 4$ nanoribbons and at zero chemical potential, and the results are shown in Fig. 4, where the analytic results are also presented. The band gap for N=3 nanoribbon is about $E_q = 2.2\,\text{eV}$, while that for N=4 is about $E_q = 2.1\,\text{eV}$ for band pair ± 2 and $E_q = 3.3\,\text{eV}$ for band pair ± 1. From the analytic results, for undoped nanoribbons there exist only interband resonances, located at $\hbar\omega = E_q/i$ for i photon process indicated by the arrows in Fig. 4. The analytic

expressions are applied to the band pair ± 1 in the extended BZ of N=3 nanoribbon, and the band pairs ± 1 and ± 2 for N=4 nanoribbons. For N=3 nanoribbons, the resonant transitions between band pair ± 1 locate at $\hbar\omega = 2.2/i\,\text{eV}$ for i-photon process (indicated by arrow i_1); while for N=4 nanoribbons, the locations become $\hbar\omega = 2.1/i\,\text{eV}$ for band pair ± 2 (indicated by arrow i_2) and $\hbar\omega = 3.3/i\,\text{eV}$ for band pair ± 1 (indicated by arrow i_1). All these peaks match the numerical results very well. There also appear additional peaks at $\hbar\omega = 2.7\,\text{eV}$ (arrow a) in Fig. 4(a), $\hbar\omega = 1.8\,\text{eV}$ (arrow b) in Fig. 4(c) and $\hbar\omega = 2.9\,\text{eV}$ (arrow c) in Fig. 4(d), which cannot be described by 1D DFs. The first two peaks (arrows a and
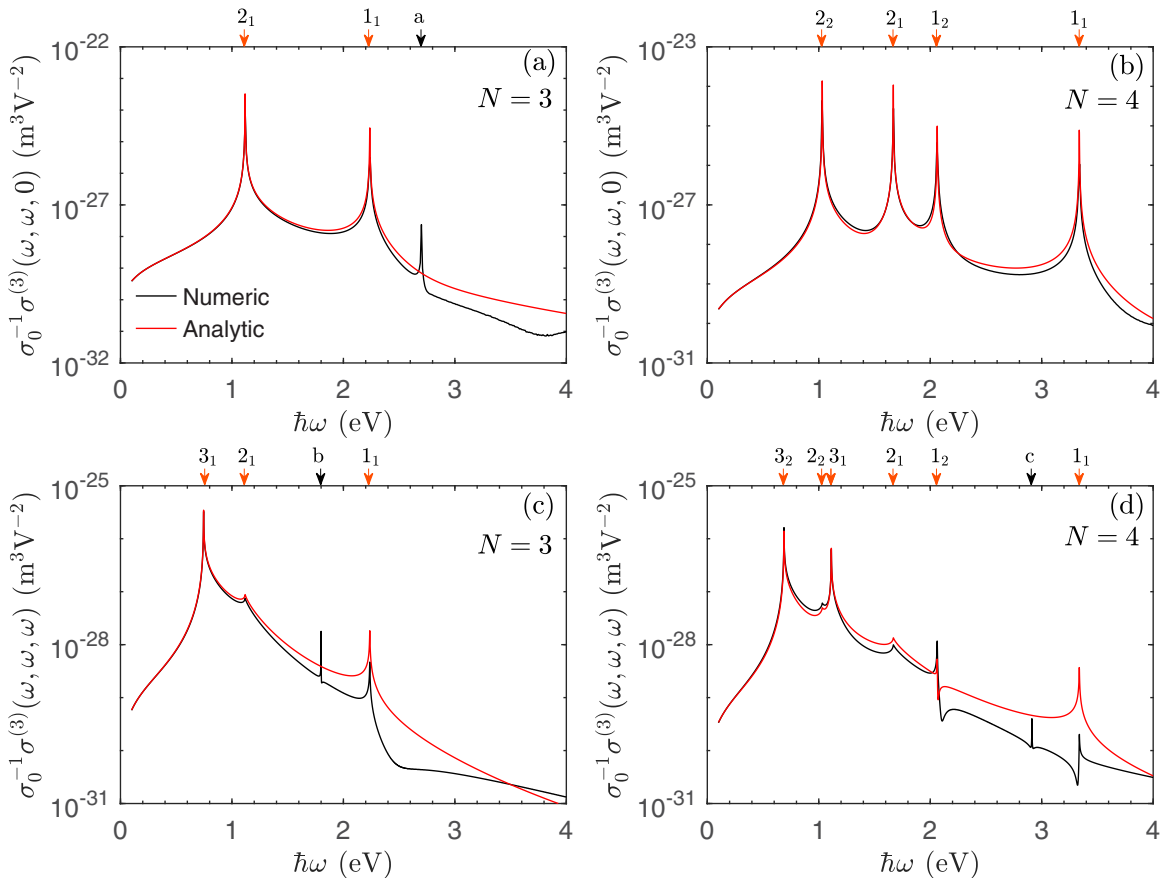

FIG. 4. Comparison of numeric and analytic result for EFISH and THG. (a), (b): EFISH; (c), (d): THG. The arrows with label i_j indicate the i-photon resonant transitions between the $\pm j$ band pair and arrows a, b, c refer to the additional peaks in numerical results.
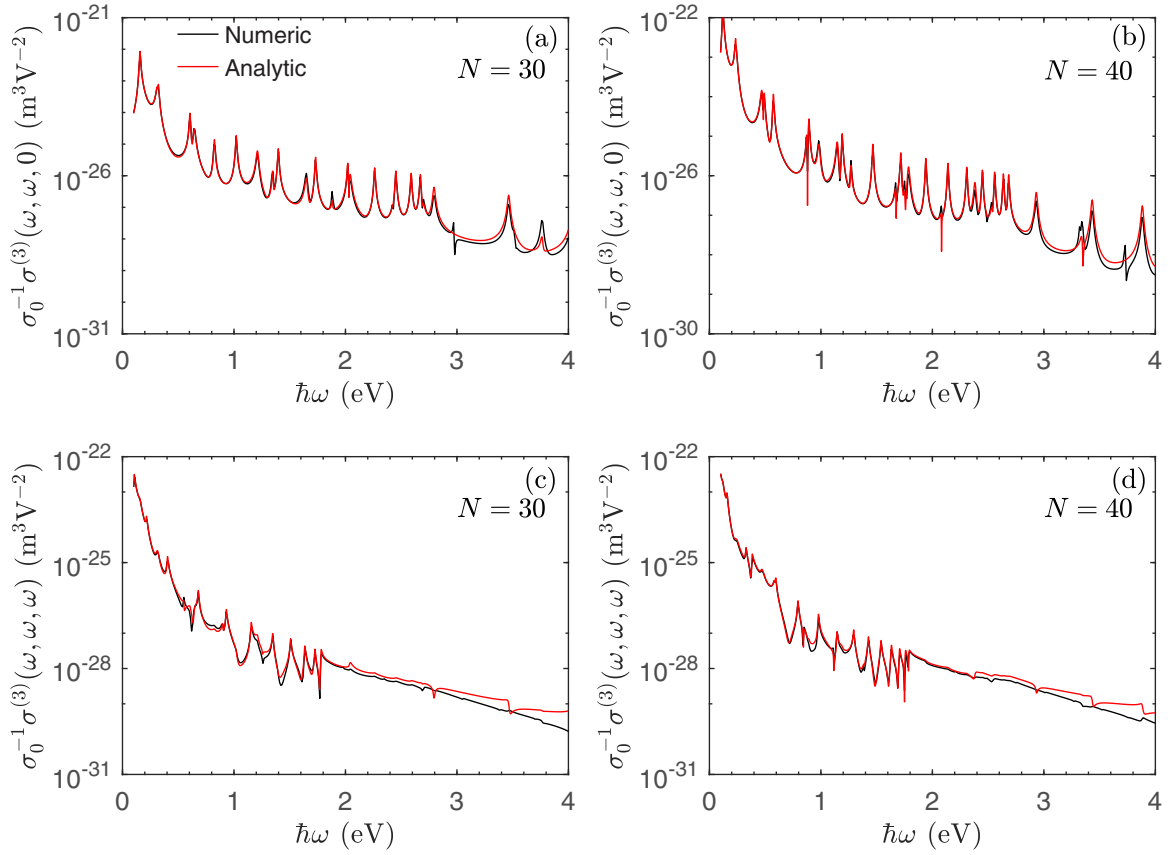
FIG. 5. Comparison of numeric and analytic results for EFISH and THG with N = 30 and N = 40. (a), (b): EFISH; (c), (d): THG.

b) arise from the two- and three-photon interband resonant transitions between the two flat bands ± 2 of N=3 nanoribbon [illustrated by the vertical arrow in Fig. 3(b)], while the third one arises from the three-photon interband resonant transition between the unfolded bands ± 3 at $k = 0$ [illustrated by the vertical arrow in Fig. 3(c)].

We estimate the effective bulk susceptibilities of these coefficients through $\chi_{\text{eff}}^{(2)}(2\omega) = E_{\text{dc}}\sigma_{\text{SHG}}^{(3)}(\omega, \omega, 0)/(-2i\omega\epsilon_0 W d)$ for EFISH and $\chi_{\text{eff}}^{(3)}(3\omega) = \sigma_{\text{THG}}^{(3)}(\omega, \omega, \omega)/(-3i\omega\epsilon_0 W d)$ for THG, where $W \approx N a_{\text{gh}}/2$ and $d = 3.3$ Å are the width and thickness of a ribbon. The width of a $N = 4$ nanoribbon is about $W \approx 5$ Å. For EFISH, the peak value around $\hbar\omega = 1.05$ eV is about $\sigma_0^{-1}|\sigma_{\text{SHG}}^{(3)}| \sim 6 \times 10^{-24}$ m^3/V^2, then the effective bulk susceptibility is $|\chi_{\text{eff}}^{(2)}| \sim 1.4 \times 10^{-8}$ m/V for a static field $E_{\text{dc}} = 10^6$ V/m. For THG, the peak value around $\hbar\omega = 0.7$ eV is about $\sigma_0^{-1}|\sigma_{\text{THG}}^{(3)}| \sim 10^{-26}$ m^3/V^2, and the effective bulk susceptibility is $|\chi_{\text{eff}}^{(3)}| \sim 10^{-16}$ m^2/V^2. Compared to the values for DFs in higher dimensions at the same photon energy, which are about 3.2×10^{-19} m^{2}V^{-2} for 2D DFs [36] and 4×10^{-21} m^{2}V^{-2} for 3D DFs [48], the effective THG susceptibility of armchair nanoribbons is about $2 - 3$ order of magnitude larger than theoretical values of graphene, and much larger than those of Dirac semimetals. The larger nonlinear susceptibility at lower dimension shows significant impact of the quantum confinement on nonlinear optical response.

We also perform such comparison in wider nanoribbons with $N = 30$ and $N = 40$, and show the results in Fig. 5. For fundamental photon energy below 2.5 eV, the analytic and numerical results agree very well. The wider ribbons include more bands, which give many resonant peaks. With further increasing the width $N \rightarrow \infty$, the armchair graphene nanoribbon becomes graphene, then we can predict that the analytic third-order optical conductivity of 1D DFs can be used to produce the third-order optical conductivity $\sigma^{(3);xxxx}$ for graphene, very similar to the case of producing the third-order optical conductivity of 3D DFs from those of a gapped 2D DFs [45]. The disagreement for photon energy higher than 2.5 eV mostly comes from the deviation of the tight binding band structure from the bands obtained by the linear dispersion Hamiltonian.

V. CONCLUSION

In conclusion, we have derived analytic expressions for the linear and third-order conductivities of one-dimensional Dirac fermions, with treating the scattering by phenomenological relaxation parameters. The spectra of third-order conductivity show very similar structure to that of two- or three-dimensional Dirac fermions, with multiple resonant divergences induced by either intraband motion or interband resonant transitions. Taking armchair graphene nanoribbon as an example, our analytic results for the field-induced second harmonic generation and third harmonic generation agree

with the numerical values pretty well. Our one-dimensional Dirac fermions model cannot be applied to another widely studied graphene nanoribbons with zigzag edges, because of the different band structure and selection rules for the optical transition between different bands [56]. Due to the existence of the nearly degenerate edge bands for zigzag graphene nanoribbons, it is interesting to study its harmonic generation using our numerical method, which is left for a future work.

Our treatment is in the single-particle approximation, which works well for two-dimensional massless Dirac fermions in graphene [9], mostly because the many-body interaction does not change the single particle dispersion relation, especially the zero value of the gap. However, the third-order nonlinearity is nonzero only for massive one-dimensional Dirac fermions, thus the many-body in-teraction, especially the excitonic effects, could be im-portant. For a real material such as graphene nanorib-bons that hosts one-dimensional Dirac fermions, there exist many bands, and how the many-body interaction be-tween them affect the optical nonlinearity deserves further investigation.

APPENDIX: EXPRESSIONS OF THE DIMENSIONLESS FUNCTIONS S_J

$$S_3(w_0; u) = \frac{1}{w_0 - u} + \frac{1}{w_0 + u}, \tag{A1a}$$

$$S_5(w; u) = \left(-3 + u\frac{\partial}{\partial u}\right)\left(\frac{1}{w - u} + \frac{1}{w + u}\right) \tag{A1b}$$

$$S_7(w, w_0; u) = 2\sum_s \frac{u^2}{w_0 - su}\frac{\partial}{\partial u}\left(\frac{1}{u}\frac{1}{w - su}\right) \tag{A1c}$$

$$S_{8a}(w, w_0, w_3; u) = \sum_s \frac{u^2}{(w_0 - su)(w_3 - su)}\frac{\partial}{\partial u}\left(\frac{1}{u}\frac{1}{w - su}\right), \tag{A1d}$$

and

$$S_2(w_3; g) = -2\left[\frac{I_6(g)}{w_3} + \frac{I_4(g)}{w_3^3} + \frac{I_2(g)}{w_3^5} + \frac{G(g; w_3)}{2w_3^6}\right], \tag{A2}$$

$$S_6(w, w_3; g) = 2\left[\frac{1}{ww_3}I_6(g) + \frac{w^2 + w_3^2}{w^3 w_3^3}I_4(g) + \frac{w^4 + w_3^2 w^2 + w_3^4}{w^5 w_3^5}I_2(g) - \frac{w_3}{2w^6(w^2 - w_3^2)}G(g; w) + \frac{w}{2w_3^6(w^2 - w_3^2)}G(g; w_3)\right], \tag{A3}$$

with $g = \max\{1, u\}$ and

$$I_4(g) = \frac{2g^3 - \sqrt{g^2 - 1}(2g^2 + 1)}{3g^3} \tag{A4}$$

$$I_6(g) = \frac{8g^5 - \sqrt{g^2 - 1}(8g^4 + 4g^2 + 3)}{15g^5}. \tag{A5}$$

The remaining S functions are

$$S_4(w_0, w_3; g) = -\left[a_1 I_6(g) + a_2 I_4(g) + a_3 I_2(g) + a_4 G(g; w_0) - a_5\frac{\partial}{\partial w_0}G(g; w_0) + a_6 G(g; w_3)\right], \tag{A6}$$

with

$$a_1 = \frac{6}{w_0 w_3}, \quad a_2 = \frac{4w_0^2(1 - w_3^2) + 2(w_0 + w_3)^2}{w_0^3 w_3^3}, \tag{A7a}$$

$$a_3 = \frac{6}{w_0 w_3^5} + \frac{4}{w_0^2 w_3^4} + \frac{2}{w_0^3 w_3^3} - \frac{4}{w_0 w_3^3} - \frac{2}{w_0^2 w_3^2} - \frac{2}{w_0^5 w_3}, \tag{A7b}$$

$$a_4 = \frac{3w_0 - 2w_3 - 2w_0^3 + w_3 w_0^2}{w_0^6(w_0 - w_3)^2}, \quad a_5 = \frac{1 - w_0^2}{w_0^5(w_0 - w_3)}, \tag{A7c}$$

$$a_6 = \frac{3w_0 - 4w_3 + 3w_3^3 - 2w_0 w_3^2}{w_3^6(w_0 - w_3)^2}, \tag{A7d}$$

and

$$S_{8b}(w, w_0, w_3; g) = 4\left[b_1 I_6(g) + b_2 I_4(g) + b_3 I_2(g) + b_4 G(g; w) - b_5 \frac{\partial}{\partial w} G(g; w) \right.$$

$$\left. + b_6 G(g; w_0) + b_7 G(g; w_3) - b_8 \frac{\partial}{\partial w_3} G(g; w_3) \right], \tag{A8}$$

with

$$b_1 = -\frac{1}{w w_0 w_3}, \quad b_2 = \frac{2w_0^2 w_3(1 + w^2) - w^2(w_0 + 2w_3)}{2w^3 w_0^3 w_3^2}, \tag{A9a}$$

$$b_3 = \frac{\left\{ \begin{array}{c} -w_3^3 w^4(2w_3 + w_0) + w_0^3 w_3 w \left[w^3 + w_3^2(w + w^3) + 4w_3^3 \right] \\ +2w_0^2 w_3^4 w^2(1 + w^2) + 2w_0^4 \left[w^4 + w_3^4(3 - w^2) + w_3^3 w \right] \end{array} \right\}}{2w^5 w_0^5 w_3^5}, \tag{A9b}$$

$$b_4 = \frac{\left\{ \begin{array}{c} w^2 \left[-12w^3 + 4w_0 w_3^2 - w w_3(11w_0 + 6w_3) + w^2(9w_0 + 16w_3) \right] \\ + \left(18w^3 - 8w_0 w_3^2 + w w_3(21w_0 + 10w_3) - w^2(15w_0 + 26w_3) \right) \end{array} \right\}}{4w^6(w - w_0)^2(w - w_3)^3}, \tag{A9c}$$

$$b_5 = \frac{(1 - w^2)(3w - 2w_3)}{4w^5(w - w_0)(w - w_3)^2}, \quad b_6 = \frac{(w - 2w_0)(1 - w_0^2)(3w_0 - 2w_3)}{4(w - w_0)^2 w_0^6(w_0 - w_3)^2}, \tag{A9d}$$

$$b_7 = \frac{\left\{ \begin{array}{c} w_3^2 \left[-w^2(w_0 - 2w_3) + 3w(w_0 - 2w_3)w_3 - 4w_0 w_3^2 + 6w_3^3 \right] \\ + w^2(3w_0 - 4w_3) + 2(4w_0 - 5w_3)w_3^2 + 3w w_3(-3w_0 + 4w_3) \end{array} \right\}}{4(w - w_3)^3(w_0 - w_3)^2 w_3^6}, \tag{A9e}$$

$$b_8 = \frac{(w - 2w_3)(1 - w_3^2)}{4(w - w_3)^2 w_3^5(w_0 - w_3)}. \tag{A9f}$$

[1] A. H. Castro Neto, F. Guinea, N. M. R. Peres, K. S. Novoselov, and A. K. Geim, Rev. Mod. Phys. **81**, 109 (2009).

[2] H. Gao, J. W. Venderbos, Y. Kim, and A. M. Rappe, Annu. Rev. Mater. Res. **49**, 153 (2019).

[3] A. Burkov, Annu. Rev. Condens. Matter Phys. **9**, 359 (2018).

[4] N. P. Armitage, E. J. Mele, and A. Vishwanath, Rev. Mod. Phys. **90**, 015001 (2018).

[5] B. Yan and C. Felser, Annu. Rev. Condens. Matter Phys. **8**, 337 (2017).

[6] J. K. Asbóth, L. Oroszlány, and A. Pályi, *A Short Course on Topological Insulators* (Springer, Cham, 2016).

[7] K. S. Novoselov, A. K. Geim, S. V. Morozov, D. Jiang, Y. Zhang, S. V. Dubonos, I. V. Grigorieva, and A. A. Firsov, Science **306**, 666 (2004).

[8] A. K. Geim, Science **324**, 1530 (2009).

[9] J. L. Cheng, J. E. Sipe, S. W. Wu, and C. Guo, APL Photonics **4**, 034201 (2019).

[10] R. Bistritzer and A. H. MacDonald, Proc. Natl. Acad. Sci. USA **108**, 12233 (2011).

[11] P. Moon and M. Koshino, Phys. Rev. B **87**, 205404 (2013).

[12] Y. Cao, V. Fatemi, S. Fang, K. Watanabe, T. Taniguchi, E. Kaxiras, and P. Jarillo-Herrero, Nature (London) **556**, 43 (2018).

[13] R. A. Muniz and J. E. Sipe, Phys. Rev. B **91**, 085404 (2015).

[14] A. Kormányos, G. Burkard, M. Gmitra, J. Fabian, V. Zólyomi, N. D. Drummond, and V. Fal'ko, 2D Mater. **2**, 022001 (2015).

[15] H. Huang, S. Zhou, and W. Duan, Phys. Rev. B **94**, 121117(R) (2016).

[16] L. Fu, C. L. Kane, and E. J. Mele, Phys. Rev. Lett. **98**, 106803 (2007).

[17] D.-H. Lee, Phys. Rev. Lett. **103**, 196804 (2009).

[18] S. M. Young, S. Zaheer, J. C. Y. Teo, C. L. Kane, E. J. Mele, and A. M. Rappe, Phys. Rev. Lett. **108**, 140405 (2012).

[19] K. Ullah, Y. Meng, Y. Sun, Y. Yang, X. Wang, A. Wang, X. Wang, F. Xiu, Y. Shi, and F. Wang, Appl. Phys. Lett. **117**, 011102 (2020).

[20] G. B. Osterhoudt, L. K. Diebel, M. J. Gray, X. Yang, J. Stanco, X. Huang, B. Shen, N. Ni, P. J. W. Moll, Y. Ran, and K. S. Burch, Nat. Mater. **18**, 471 (2019).

[21] K. Nakada, M. Fujita, G. Dresselhaus, and M. S. Dresselhaus, Phys. Rev. B **54**, 17954 (1996).

[22] Y.-W. Son, M. L. Cohen, and S. G. Louie, Phys. Rev. Lett. **97**, 216803 (2006).

[23] C. Attaccalite, E. Cannuccia, and M. Grüning, Phys. Rev. B **95**, 125403 (2017).

[24] E. S. Azarova, G. M. Maksimova, and V. A. Burdov, Phys. E **106**, 140 (2019).

[25] S. Yue, H. Zhou, Y. Feng, Y. Wang, Z. Sun, D. Geng, M. Arita, S. Kumar, K. Shimada, P. Cheng, L. Chen, Y. Yao, S. Meng, K. Wu, and B. Feng, Nano Lett. **22**, 695 (2022).

[26] Y. I. Dakhovskii and K. A. Pronin, Synth. Met. **54**, 295 (1993).

[27] C. L. Kane and E. J. Mele, Phys. Rev. Lett. **95**, 146802 (2005).

[28] I. K. Drozdov, A. Alexandradinata, S. Jeon, S. Nadj-Perge, H. Ji, R. J. Cava, B. Andrei Bernevig, and A. Yazdani, Nat. Phys. **10**, 664 (2014).

[29] R. R. Nair, P. Blake, A. N. Grigorenko, K. S. Novoselov, T. J. Booth, T. Stauber, N. M. R. Peres, and A. K. Geim, Science **320**, 1308 (2008).

[30] F. de Juan, A. G. Grushin, T. Morimoto, and J. E. Moore, Nat. Commun. **8**, 15995 (2017).

[31] K. F. Mak, M. Y. Sfeir, Y. Wu, C. H. Lui, J. A. Misewich, and T. F. Heinz, Phys. Rev. Lett. **101**, 196405 (2008).

[32] Y.-C. Chang, C.-H. Liu, C.-H. Liu, Z. Zhong, and T. B. Norris, Appl. Phys. Lett. **104**, 261909 (2014).

[33] E. Hendry, P. J. Hale, J. Moger, A. K. Savchenko, and S. A. Mikhailov, Phys. Rev. Lett. **105**, 097401 (2010).

[34] J. Ma, Q. Gu, Y. Liu, J. Lai, P. Yu, X. Zhuo, Z. Liu, J.-H. Chen, J. Feng, and D. Sun, Nat. Mater. **18**, 476 (2019).

[35] S. A. Mikhailov, Europhys. Lett. **79**, 27002 (2007).

[36] J. L. Cheng, N. Vermeulen, and J. E. Sipe, New J. Phys. **16**, 053014 (2014); **18**, 029501 (2016).

[37] Y. Zhong, W. Feng, Z. Liu, C. Zhang, and J. C. Cao, Phys. B: Condens. Matter **555**, 81 (2019).

[38] S. J. Brun and T. G. Pedersen, Phys. Rev. B **91**, 205405 (2015).

[39] T. Jiang, D. Huang, J. Cheng, X. Fan, Z. Zhang, Y. Shan, Y. Yi, Y. Dai, L. Shi, K. Liu, C. Zeng, J. Zi, J. E. Sipe, Y.-R. Shen, W.-T. Liu, and S. Wu, Nat. Photonics **12**, 430 (2018).

[40] G. Soavi, G. Wang, H. Rostami, D. G. Purdie, D. De Fazio, T. Ma, B. Luo, J. Wang, A. K. Ott, D. Yoon, S. A. Bourelle, J. E. Muench, I. Goykhman, S. Dal Conte, M. Celebrano, A. Tomadin, M. Polini, G. Cerullo, and A. C. Ferrari, Nat. Nanotechnol. **13**, 583 (2018).

[41] K. Yu, N. Van Luan, T. Kim, J. Jeon, J. Kim, P. Moon, Y. H. Lee, and E. J. Choi, Phys. Rev. B **99**, 241405(R) (2019).

[42] K. J. A. Ooi, Y. S. Ang, Q. Zhai, D. T. H. Tan, L. K. Ang, and C. K. Ong, APL Photonics **4**, 034402 (2019).

[43] P. Cheng, C. Zhang, Y. Liu, X. Yuan, F. Song, Q. Sun, P. Zhou, D. W. Zhang, and F. Xiu, New J. Phys. **18**, 083003 (2016).

[44] V. Kumar, J. Electron. Mater. **50**, 3773 (2021).

[45] J. L. Cheng, N. Vermeulen, and J. E. Sipe, Phys. Rev. B **92**, 235307 (2015).

[46] H. Rostami and M. Polini, Phys. Rev. B **93**, 161411(R) (2016).

[47] F. Yang, W. Song, F. Meng, F. Luo, S. Lou, S. Lin, Z. Gong, J. Cao, E. S. Barnard, E. Chan, L. Yang, and J. Yao, Matter **3**, 1361 (2020).

[48] J. L. Cheng, J. E. Sipe, and S. W. Wu, ACS Photonics **7**, 2515 (2020).

[49] T. Zhang, K. J. A. Ooi, W. Chen, L. K. Ang, and Y. S. Ang, Opt. Express **27**, 38270 (2019).

[50] D. Kaplan, T. Holder, and B. Yan, Phys. Rev. Research **4**, 013209 (2022).

[51] Y. Xiong, L. kun Shi, and J. C. W. Song, 2D Mater. **8**, 035008 (2021).

[52] C. J. Tabert and E. J. Nicol, Phys. Rev. B **86**, 075439 (2012).

[53] J. L. Cheng, N. Vermeulen, and J. E. Sipe, Phys. Rev. B **91**, 235320 (2015).

[54] E. J. König, A. Levchenko, and N. Sedlmayr, Phys. Rev. B **93**, 235160 (2016).

[55] K. Wakabayashi, K.-I. Sasaki, T. Nakanishi, and T. Enoki, Sci. Techn. Adv. Mater. **11**, 054504 (2010).

[56] C. Salazar, J. L. Cheng, and J. E. Sipe, Phys. Rev. B **93**, 075442 (2016).